
EFFECT OF INNER CRUST EOS ON NEUTRON STAR MASS AND RADII

A PREPRINT

Ishfaq A. Rather

Department of Physics Aligarh Muslim University, Aligarh-202002, India
ishfaqrather81@gmail.com

A. A. Usmani

Department of Physics Aligarh Muslim University, Aligarh-202002, India

S. K. Patra

Institute of Physics, Bhubaneswar 751005, India
Homi Bhabha National Institute, Training School Complex, Anushakti Nagar, Mumbai 400085, India

September 29, 2020

ABSTRACT

The neutron star maximum mass and the radius are investigated within the framework of relativistic mean-field (RMF) model. The variation in the radius at the canonical mass, $R_{1.4}$, using different inner crust equation of state (EoS) with different symmetry energy slope parameter is also studied. It is found that although the NS maximum mass and the corresponding radius do not vary much with different slope parameter inner crust EoS, the radius at $1.4M_{\odot}$ follows a linear correlation with the symmetry energy slope parameter for all core parameter sets.

Keywords Unified EoS · Inner crust · Neutron star

1 Introduction

The structure and the properties of Neutron Stars (NS) have been studied effectively from experimental as well as theoretical models. Such studies reveal the inner structure of NS and the presence of exotic phases. The results obtained from the astrophysical observations require several theoretical inputs for the interpretation. A coextensive effort from theory and experiments have improved and provided new insights into the field. The recently observed Gravitational Waves GW170817 [1, 2] and GW190425 [3] have constrained the NS maximum mass and radius. The presence of exotic phases like quarks inside NS has also been observed recently [4]. After the discovery of gravitational wave GW170817, more theoretical work has been done to understand the relation between EoS and NS properties through various aspects like a phase transition, symmetry energy [5, 6, 7, 8, 9, 10, 11, 12, 13]. However, there are still numerous fundamental problems related to the matter under extreme conditions that are yet to be answered. The most important one is the unified theory which can describe the overall structure of a NS, from the outer crust to the inner core.

The structure and the properties of a NS are determined by the Equation of State (EoS) which describes the state of matter under given physical conditions. The discovery of massive neutron stars provide constrain on NS maximum mass and radius [14, 15, 16]. To determine the pressure and the energy density of a NS matter, the isospin asymmetry and the binding energy act as the key inputs. The symmetry energy $S(\rho)$ and its derivatives ($L_{sym}, K_{sym}, Q_{sym}$) affect the EoS and have been used to constrain the EoS near the saturation density. The density-dependent symmetry energy has a strong correlation between the pressure at saturation density and its radius inside a NS [17]. It has been shown [18, 19] that the slope parameter L_{sym} is strongly correlated to the neutron skin thickness. A higher

L_{sym} value describes neutron matter with higher pressure and hence thicker neutron skin [20, 21, 22]. The curvature parameter K_{sym} determines the crust-core transition density and the gravitational binding energy of the NS [23]. The skewness parameter Q_{sym} has a large saturation in its value due to different values from various models. The skewness parameter is related to the nuclear incompressibility of the system [24]. All these quantities affect the EoS directly or indirectly.

The unified EoS describes the neutron star from its outer crust to the inner core. However, a unified EoS is generally not available. Hence the complete EoS is divided into three different phases: the outer crust phase, the inner crust, and the core phase. It has been shown [25, 26] that the neutron star properties like mass and radius do not depend upon the outer crust EoS, but a particular choice of inner crust EoS and the matching of inner crust to the core EoS is critical and the variations larger than 0.5 km have been obtained for a $1.4 M_{\odot}$. For the outer crust which lies in the density range 10^4 - 10^{11} g/cm³, the Baym-Pethick-Sutherland (BPS) EoS [27], the Haensel-Pichon (HP) EoS [28] are widely used in the literature. Both these EoS do not affect the mass and radius of a neutron star. For the matter beyond the neutron drip line ranging from density 10^{11} - 10^{14} g/cm³, the inner crust EoS follows. The Baym-Bethe-Pethick (BBP) EoS [29] is usually used. However to avoid the large uncertainties in mass and radius of a neutron star, studies have shown that for the complete unified EoS, the inner crust EoS should be either from the same model as core EoS or the symmetry energy slope parameter should match [26, 30]. Thus a proper choice of inner crust EoS will determine the true value of neutron star mass and radius.

This paper is organized as follows. In section 2, we explain the relativistic-mean field formalism to the study of the EoS. Section 3 discusses the nuclear matter properties for parameter sets used. The unified EoS by combining the outer crust, inner crust, and the core EoS will be discussed in section 3. The mass-radius profile for the neutron star matter with different EoSs is also discussed. Finally, the summary and conclusions are outlined in section 4.

2 Theory and Formalism

In this section, we summarize the formulations of our EoS for nuclear matter. The Relativistic Mean Field (RMF) theory in which the nucleons interact through the meson exchange is adopted. The simplest relativistic Lagrangian contains the contribution from σ , ω , and ρ mesons without any cross-coupling between them [31]. The prediction of large nuclear matter incompressibility [32] by this model was reduced to an acceptable range by the addition of self-coupling terms [33]. The addition of other self- and cross-couplings improved the nuclear matter properties. The Effective field theory motivated RMF (E-RMF) is an extension to the basic RMF theory in which all possible self- and cross-couplings between the mesons are included [34, 35, 36]. The E-RMF Lagrangian used in the present work, which contains the contribution from σ -, ω - mesons up to 4th order expansion, and ρ - and δ - mesons up to 2nd order are given by [37]

$$\begin{aligned}
\mathcal{L} = & \sum_{\alpha=n,p} \bar{\psi}_{\alpha} \left\{ \gamma_{\mu} (i\partial^{\mu} - g_{\omega}\omega^{\mu} - \frac{1}{2}g_{\rho}\tau_{\alpha}\cdot\rho^{\mu}) - (M - g_{\sigma}\sigma) \right. \\
& \left. - g_{\delta}\tau_{\alpha}\cdot\delta \right\} \psi_{\alpha} + \frac{1}{2}\partial^{\mu}\sigma\partial_{\mu}\sigma - \frac{1}{2}m_{\sigma}^2\sigma^2 + \frac{\zeta_0}{4!}g_{\omega}^2(\omega^{\mu}\omega_{\mu})^2 \\
& - g_{\sigma}\frac{m_{\sigma}^2}{M}\left(\frac{k_3}{3!} + \frac{k_4}{4!}\frac{g_{\sigma}}{M}\sigma\right)\sigma^3 + \frac{1}{2}m_{\omega}^2\omega^{\mu}\omega_{\mu} - \frac{1}{4}F^{\mu\nu}F_{\mu\nu} \\
& + \frac{1}{2}\frac{g_{\sigma}\sigma}{M}\left(\eta_1 + \frac{\eta_2}{2}\frac{g_{\sigma}}{M}\sigma\right)m_{\omega}^2\omega^{\mu}\omega_{\mu} + \frac{1}{2}\eta_{\rho}\frac{m_{\rho}^2}{M}g_{\sigma}\sigma(\rho^{\mu}\cdot\rho_{\mu}) \\
& + \frac{1}{2}m_{\rho}^2\rho^{\mu}\cdot\rho_{\mu} - \frac{1}{4}R^{\mu\nu}\cdot R_{\mu\nu} - \Lambda_{\omega}g_{\omega}^2g_{\rho}^2(\omega^{\mu}\omega_{\mu})(\rho^{\mu}\cdot\rho_{\mu}) \\
& + \frac{1}{2}\partial^{\mu}\delta\partial_{\mu}\delta - \frac{1}{2}m_{\delta}^2\delta^2,
\end{aligned} \tag{1}$$

where ψ is the nucleonic field and M is the nucleonic mass. m_{σ} , m_{ω} , m_{ρ} , and m_{δ} are the masses and g_{σ} , g_{ω} , g_{ρ} , and g_{δ} are the coupling constants of σ , ω , ρ , and δ mesons respectively. The Euler-Lagrangian equations of motion for the meson fields are obtained using the relativistic mean-field approximation [8]. The expression for the energy density and pressure are obtained from the given Lagrangian using energy-momentum tensor relation [38]. The expression for energy density and pressure are given by [8].

3 Results and Discussion

To study the effect of crust EoS on neutron star properties, we have chosen several parameter sets to construct the core EoS. Since the outer crust EoS does not affect the neutron star maximum mass and radius, therefore the use of several EoSs for outer crust will provide no new information regarding the NS. Hence the BPS EoS [27] has been used for the outer crust part. For the inner crust part, the relativistic mean-field model with constant couplings, non-linear terms [39], and density-dependent couplings [40] have been used. These include NL3 [41] set with non-linear σ terms, TM1 [42] with non-linear σ and ω terms, NL3 $\omega\rho$ [43, 22] which includes the non-linear $\omega\rho$ terms in addition to the previous couplings, FSU [44] and IU-FSU [45], and the density-dependent DD-ME2 [46] and DD-ME δ [47].

The nuclear matter properties at saturation density for the above considered crust EoSs are shown in table 1. The symmetry energy slope parameter L_{sym} of the given sets lies in the range 47-118 MeV. We have considered these sets for the inner crust part to determine the variation in the maximum mass and the corresponding radius of a neutron star.

Table 1: Nuclear matter properties for the crust EoS at saturation density (ρ_0), energy (E_0), symmetry energy (S), slope parameter (L_{sym}), incompressibility coefficient (K), and skewness parameter (Q_{sym}). All the values are in MeV except for the (ρ_0) which is in fm^{-3} .

Model	ρ_0	E_0	S	L_{sym}	K	Q_{sym}
NL3	0.148	-16.24	37.3	118.3	270.7	203
TM1	0.145	-16.26	36.8	110.6	280.4	-295
FSU	0.148	-16.30	32.6	60.5	230.0	-523
IU-FSU	0.155	-16.40	31.3	47.2	213.2	-288
NL3 $\omega\rho$	0.148	-16.30	31.7	55.2	272.0	203
DD-ME2	0.152	-16.14	32.3	51.4	250.8	478
DD-ME δ	0.152	-16.12	32.4	52.9	219.1	-741

The E-RMF formalism is used to construct the core EoS. We covered a wide range of models containing only σ self-coupling terms to the models with all types of self- and cross-couplings along with the δ meson inclusion. NL3 [41], TM1 [42], IU-FSU [48], IOPB-I [8], and G3 [36] parameter sets are used to study the neutron star core. All the coupling constants and the meson masses for the above parameter sets are given in [42, 48, 8].

The unified EoSs consisting of the outer crust, the inner crust, and the core are constructed using the above defined parameter sets. The unified EoS follows as: BPS (for the outer crust)+ BBP, NL3, TM1, NL3 $\omega\rho$, FSU, IU-FSU, DD-ME2, and DD-ME δ (for the inner crust)+ NL3, TM1, IU-FSU, IOPB-I, and G3 (for the core). The unified EoS without inner crust is also constructed to see the impact of inner crust on NS properties. The different unified EoSs produced are shown in figure 1.

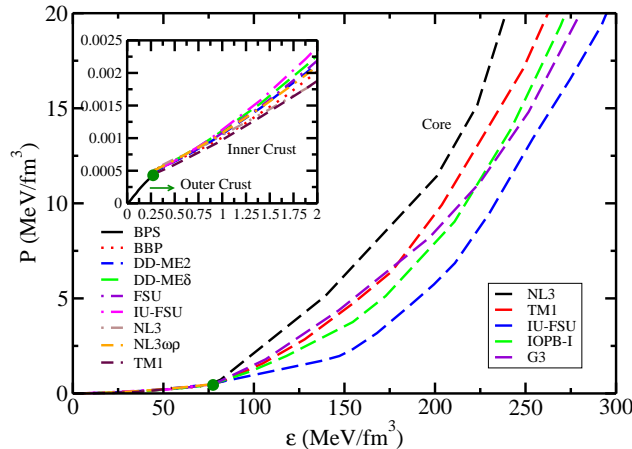


Figure 1: Unified EoS with different inner crust and core EoS. The inset shows the matching of outer crust with the inner crust.

The NL3 parameter set produces stiff EoS as compared to other parameter sets. IU-FSU produces soft EoS among all. G3 set produces soft EoS as compared to NL3, TM1 and IOPB-I at both low and high energy densities. Among the inner crust EoS, NL3 and TM1 set produce soft EoS at very low density and become stiff as the density increases. IU-FSU initially produces stiff EoS but becomes soft at higher energy density ($\mathcal{E} \approx 45 \text{ MeV}/\text{fm}^3$).

To determine the maximum mass and the corresponding radius of a stationary and spherical neutron stars obtained using different EoSs, we use the Tolman–Oppenheimer–Volkoff (TOV) equations [49, 50].

$$\frac{dP(r)}{dr} = -\frac{[\mathcal{E}(r) + P(r)][M(r) + 4\pi r^3 P(r)]}{r^2(1 - 2M(r)/r)} \quad (2)$$

and

$$\frac{dM(r)}{dr} = 4\pi r^2 \mathcal{E}(r) \quad (3)$$

Here $M(r)$ is the gravitational mass. For the given boundary conditions $P(0) = P_c$, $M(0) = 0$, with P_c being the central pressure, the equations (2) and (3) are solved to obtain the NS properties.

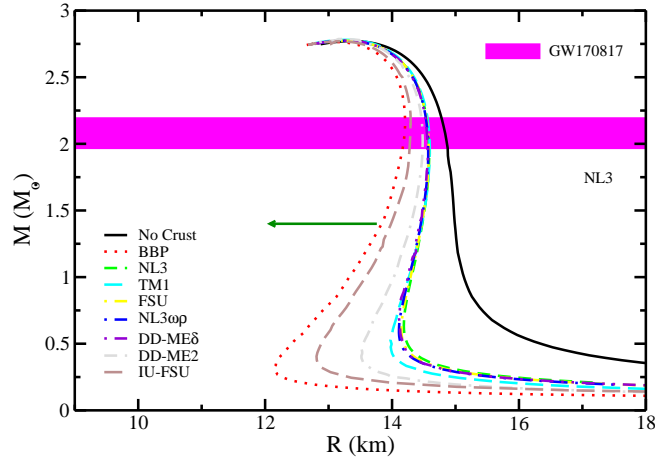


Figure 2: Mass-Radius profile for NL3 core with different inner crust EoS. The recent constrains on the mass [51] and radius [9] of NS are also shown.

Figure 2 shows the mass-radius relation for a NS with NL3 core EoS. The violet band represents the maximum mass range for a non-rotating NS [14, 51, 52]. This band also satisfies the precisely measured masses of binary millisecond pulsar PSR J1614-2230 ($1.97 \pm 0.04 M_\odot$) [16] and PSR J0348+0432 ($2.01 \pm 0.04 M_\odot$) [14]. The green arrow represents the radius at the canonical mass of a NS which shows that the maximum value of radius should be $R_{1.4} \leq 13.76 \text{ km}$ [9]. The constraints on the maximum mass show that the theoretical prediction of a NS maximum mass should reach the limit $\approx 2.0 M_\odot$. From figure 2, it is clear that the NS maximum mass produced using different inner crust EoS lies in the range $2.764\text{-}2.787 M_\odot$. The corresponding radius varies from $13.027\text{-}13.378 \text{ km}$. The radius at canonical mass is much more affected than the radius at maximum mass. For a NS without inner crust, the radius at the canonical mass is found out to be $R_{1.4} = 14.987 \text{ km}$. With the addition of the inner crust, the radius decreases from $14.479\text{-}13.834 \text{ km}$. The smallest radius is produced by using BBP as inner crust EoS which is also close to the radius predicted by GW170817. The NL3 set has higher value of symmetry energy slope parameter $L_{sym} = 118.3 \text{ MeV}$, while as IU-FSU has smallest value $L_{sym} = 47.2 \text{ MeV}$. The low value slope parameter set (IU-FSU) produces a smaller radius at the canonical mass as compared to the higher value L_{sym} set (NL3) as can be seen in the figure. Thus we see that the $R_{1.4}$ has a significant relation with the slope parameter. This is consistent with the work in ref. [9, 11].

The Mass-Radius profile for TM1 and IU-FSU parameter sets are shown in figure 3. For TM1 core EoS with different inner crust EoS, the maximum mass and the corresponding radius lie in the range $2.133\text{-}2.167 M_\odot$ and $12.206\text{-}12.725 \text{ km}$, respectively as shown in figure 3a. The radius at the canonical mass varies from $13.963\text{-}15.549 \text{ km}$ with a 15.549 km radius produced without using the inner crust. As seen in the figure, although every EoS for TM1 core along with different inner crust satisfies the mass constrain from recently observed gravitational wave data GW170817, no

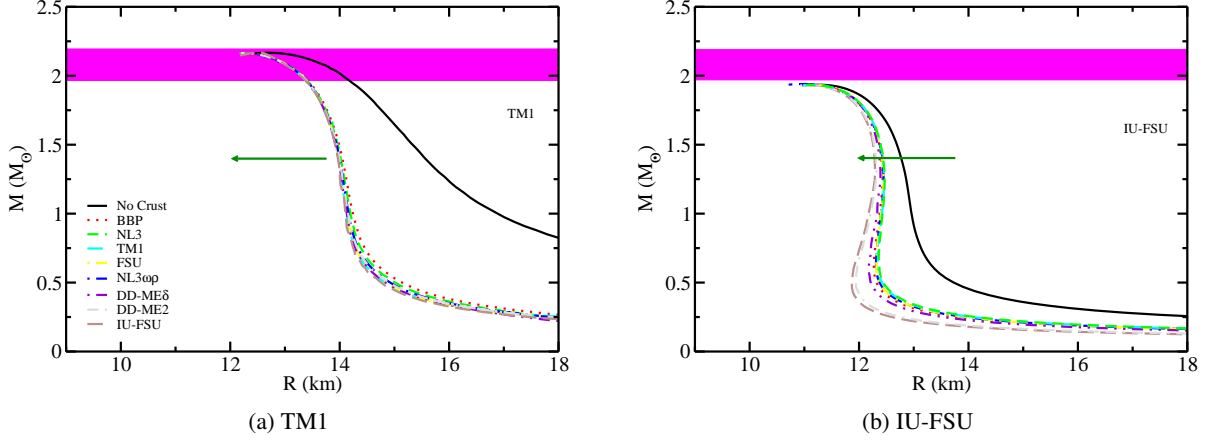


Figure 3: Same as figure 2, but for TM1 and IU-FSU core EoS.

such EoS satisfies the radius constrain. For IU-FSU core EoS, as shown in the figure 3b, the maximum mass and radius vary from $1.931\text{-}1.940 M_{\odot}$ and $11.012\text{-}11.263$ km, respectively. The radius at the canonical mass varies from $11.012\text{-}11.263$ km.

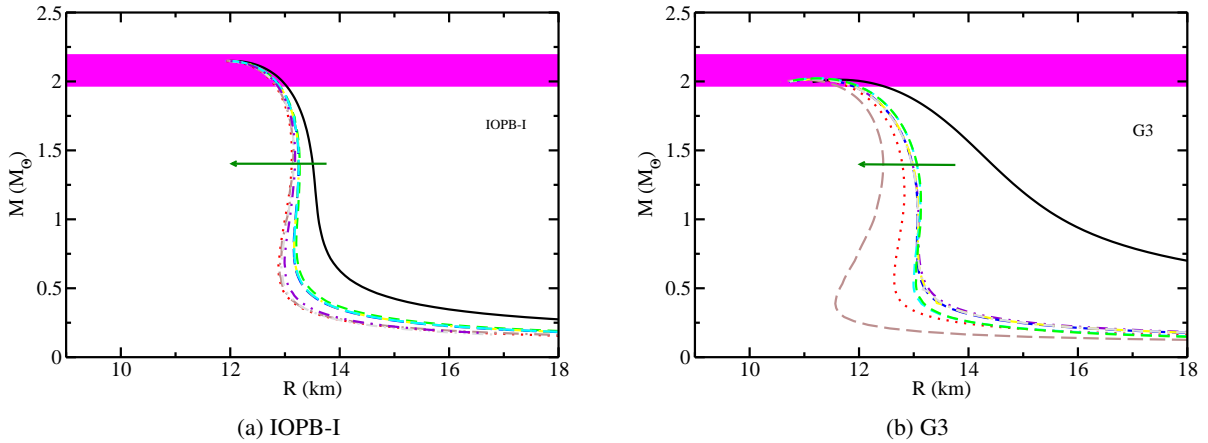


Figure 4: Same as figure 2, but for IOPB-I and G3 core EoS.

Figure 4 shows the MR profile for IOPB-I and G3 core EoS. For IOPB-I set, the maximum mass varies from $2.147\text{-}2.151 M_{\odot}$ and the radius $11.872\text{-}12.029$ km. $R_{1.4}$ varies from $13.161\text{-}13.508$ km. Similar results follow for G3 EoS, where the NS maximum mass and the corresponding radius vary slightly with different inner crust EoS. However, as usual, the radius $R_{1.4}$ varies from $12.441\text{-}14.393$ km.

From the above MR relations, we see that the maximum mass and the radius do not change by using the inner crust with different slope parameters. However, the radius at canonical mass increases with an increase in the symmetry energy slope parameter L_{sym} .

The relation between radius at the canonical mass, $R_{1.4}$, and the symmetry energy slope parameter L_{sym} for all core parameter sets are plotted in figure 5. It is clear from the plot that there is a linear correlation between $R_{1.4}$ and L_{sym} . For NL3 parameter set, the radius can be expressed as $R_{1.4} = 13.875 + 0.005221L_{sym}$ with correlation coefficient $R = 0.925$. Similar pattern follows for all other parameter sets. A larger L_{sym} results in a larger radius at the canonical mass.

Table 2 shows the deviation in the NS maximum mass, the corresponding radius, and the radius at the canonical mass for the given parameter sets. It is clear that the variation in the maximum mass and the corresponding radius are very small for EoSs, but the radius at $1.4 M_{\odot}$ is highly impacted by the inner crust EoS. For NL3 core EoS, the variation in the radius at $R_{1.4}$ is maximum for BBP inner crust $\approx 7.7\%$ which is around 2 km. The maximum variation in the radius, $R_{1.4}$, is seen for TM1 and G3 core EoSs which occur due to IU-FSU inner crust EoS. Such large deviations

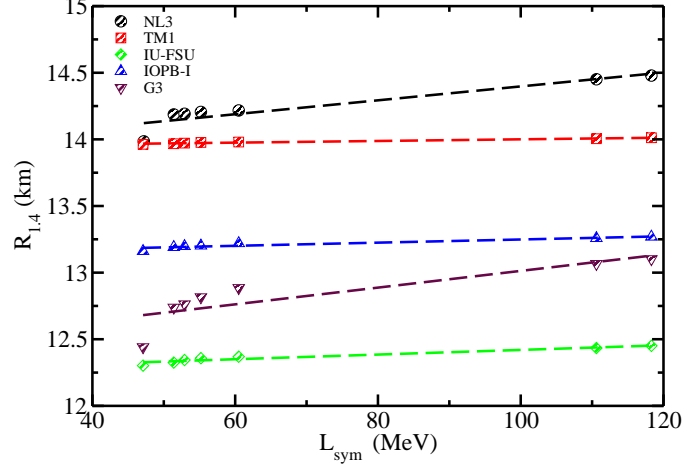


Figure 5: The relation between slope parameter and $R_{1.4}$ for NL3, TM1, IU-FSU, IOPB-I, and G3 parameter sets. The dashed lines are the fitted lines.

Table 2: Variation (in percent) in the maximum mass, corresponding radius, and the radius at $1.4M_{\odot}$ of a NS without inner crust and the corresponding inner crust.

Model		BBP	IU-FSU	DD-ME2	DD-ME δ	NL3 $\omega\rho$	FSU	TM1	NL3
NL3	ΔM_{max}	0.25	0.14	0.11	0.07	0.11	0.11	0.32	0.58
	ΔR_{max}	1.90	2.62	0.87	1.22	0.93	0.79	0.73	1.19
	$\Delta R_{1.4}$	7.71	6.74	5.31	5.29	5.24	5.17	3.62	3.44
TM1	ΔM_{max}	0.14	1.57	0.88	0.83	0.14	1.57	0.18	0.42
	ΔR_{max}	3.59	0.32	0.91	0.98	3.76	0.32	3.54	2.36
	$\Delta R_{1.4}$	9.72	10.25	10.21	10.17	10.14	10.10	9.95	9.92
IU-FSU	ΔM_{max}	0.10	0.00	0.05	0.26	0.10	0.05	0.15	0.21
	ΔR_{max}	1.35	2.07	1.41	2.23	1.25	1.26	1.71	1.79
	$\Delta R_{1.4}$	2.95	3.74	3.56	3.44	3.31	3.23	2.75	2.51
IOPB-I	ΔM_{max}	0.09	0.09	0.04	0.04	0.04	0.09	0.04	0.04
	ΔR_{max}	1.11	1.17	0.66	0.61	0.73	0.54	0.92	1.30
	$\Delta R_{1.4}$	2.81	2.66	2.37	2.35	2.32*	2.17	1.81	1.79
G3	ΔM_{max}	0.05	0.00	0.15	0.20	0.15	0.30	0.04	0.50
	ΔR_{max}	3.94	5.74	4.02	3.79	4.24	3.28	0.92	3.50
	$\Delta R_{1.4}$	11.22	13.56	11.58	11.32	10.94	10.52	9.27	8.96

in the radius, $R_{1.4}$ show that a proper choice of inner crust EoS is important to calculate the mass and radius of a NS with small uncertainties in these values. Thus the crust-core transition allows the construction of a stellar EoS and a precise measurement of the NS maximum mass and radius.

The constraints on the inner crust EoS of a NS and the proper matching of inner crust with core EoS is helpful in considering the nuclear and astrophysical applications of the RMF model. A core EoS with a smaller symmetry energy slope parameter implies small symmetry energy at high densities [53]. For a model with higher symmetry energy at sub-saturation density, the inner crust properties of a NS are affected in addition to the pasta phases as shown in refs. [54, 55]. Studies have shown that for a complete unified EoS, the inner crust part should either be from the same model or the symmetry energy slope parameter should match. However, as we have seen in the above plots, the inner crust EoS with smaller slope parameter L_{sym} predicts a smaller radius at $1.4 M_{\odot}$ as compared to the one with large L_{sym} . The same trend is followed by all parameter sets used for the core.

4 Summary and conclusion

The NS properties like mass and radius were investigated using the relativistic mean-field (RMF) model. To study the effect of symmetry energy and its slope parameter on a neutron star, we used inner crust EoSs with different symmetry

energy slope parameters. For the outer crust, the BPS EoS is used for all sets as the outer crust part doesn't affect the NS maximum mass and radius. For the inner crust part, we used NL3, TM1, FSU, NL3 $\omega\rho$, DD-ME δ , DD-ME2, and IU-FSU parameter sets whose slope parameter varies from 118.3-47.2 MeV. For the core part, NL3, TM1, IU-FSU, IOPB-I, and G3 parameter sets are used. The unified EoS are constructed by properly matching the inner crust EoS with outer crust and core EoS. The EoSs constructed for the spherical and symmetrical NS under charge neutral and β -equilibrium conditions were taken as the input into the TOV equation to obtain NS properties. It is seen that although the NS maximum mass and the corresponding radius do not change by a large amount, the radius at the canonical mass, $R_{1.4}$ are largely impacted by using inner crust EoSs with different symmetry energy slope parameter. By varying the slope parameter from low to high values, the radius $R_{1.4}$ also increases. Different parameter sets for core EoS were used to see if they predicted a different behavior between $R_{1.4}$ and L_{sym} . Also, the variation in the NS maximum mass, radius, and the radius at $1.4M_{\odot}$ are calculated and the variation of about 2 km is found in the radius at the canonical mass.

There are several different aspects that need to be further studied in the current work. A unified EoS with both crust and core part described by the same parameter set with different slope parameter L_{sym} will be a better investigation to see how the radius at canonical mass behaves. The variation in the tidal deformability of a NS with different symmetry energy slope parameter inner crust will provide more new insights into this work.

References

- [1] B. P. Abbott and et al. *Phys. Rev. Lett.*, 119:161101, Oct 2017.
- [2] B. P. Abbott and et al. *Phys. Rev. Lett.*, 121:161101, Oct 2018.
- [3] B. P. Abbott and et al. *The Astrophys. J.*, 892:L3, mar 2020.
- [4] E. Annala, T. Gorda, and et al. *Nat. Phys.*, 16:907–910, sep 2020.
- [5] Eemeli Annala, Tyler Gorda, Alekski Kurkela, and Alekski Vuorinen. *Phys. Rev. Lett.*, 120:172703, Apr 2018.
- [6] Vasileios Paschalidis, Kent Yagi, David Alvarez-Castillo, David B. Blaschke, and Armen Sedrakian. *Phys. Rev. D*, 97:084038, Apr 2018.
- [7] Tuhin Malik, N. Alam, M. Fortin, C. Providência, B. K. Agrawal, T. K. Jha, Bharat Kumar, and S. K. Patra. *Phys. Rev. C*, 98:035804, Sep 2018.
- [8] Bharat Kumar, S. K. Patra, and B. K. Agrawal. *Phys. Rev. C*, 97:045806, Apr 2018.
- [9] F. J. Fattoyev, J. Piekarewicz, and C. J. Horowitz. *Phys. Rev. Lett.*, 120:172702, Apr 2018.
- [10] Elias R. Most, Lukas R. Weih, Luciano Rezzolla, and Jürgen Schaffner-Bielich. *Phys. Rev. Lett.*, 120:261103, Jun 2018.
- [11] Yeunhwan Lim and Jeremy W. Holt. *Phys. Rev. Lett.*, 121:062701, Aug 2018.
- [12] *Int. J. Mod. Phys. E*, 29(07):2050044, 2020.
- [13] Ishfaq A Rather, A A Usmani, and S K Patra. *J. Phys. G Nucl. Part. Phys.*, 47(10):105104, sep 2020.
- [14] John Antoniadis and et al. *Science*, 340(6131), 2013.
- [15] Emmanuel Fonseca and et al. *Astrophys. J.*, 832(2):167, dec 2016.
- [16] P. B. Demorest, T. Pennucci, S. M. Ransom, M. S. E. Roberts, and J. W. T. Hessels. *Nature*, 467(7319):1081–1083, October 2010.
- [17] J. M. Lattimer and M. Prakash. *The Astrophys. J.*, 550(1):426–442, 2001.
- [18] B. Alex Brown. *Phys. Rev. Lett.*, 85:5296–5299, Dec 2000.
- [19] S. Typel and B. Alex Brown. *Phys. Rev. C*, 64:027302, Jun 2001.
- [20] X. Roca-Maza, M. Centelles, X. Viñas, and M. Warda. *Phys. Rev. Lett.*, 106:252501, Jun 2011.
- [21] R.J. Furnstahl. *Nucl. Phys. A*, 706(1):85 – 110, 2002.
- [22] C. J. Horowitz and J. Piekarewicz. *Phys. Rev. Lett.*, 86:5647–5650, Jun 2001.
- [23] M.B. Tsang, W.G. Lynch, P. Danielewicz, and C.Y. Tsang. *Phys. Lett. B*, 795:533 – 536, 2019.
- [24] S. Typel. *Particles*, 1:3, 2018.
- [25] M. Fortin, C. Providência, Ad. R. Raduta, F. Gulminelli, J. L. Zdunik, P. Haensel, and M. Bejger. *Phys. Rev. C*, 94:035804, Sep 2016.

- [26] H. Pais and C. Providência. *Phys. Rev. C*, 94:015808, Jul 2016.
- [27] Gordon Baym, Christopher Pethick, and Peter Sutherland. *Astrophys. J.*, 170:299–317, 1971.
- [28] P. Haensel and B. Pichon. *Astron. Astrophys.*, 283(1):313–318, March 1994.
- [29] Gordon Baym, Hans A. Bethe, and Christopher J Pethick. *Nucl. Phys. A*, 175(2):225 – 271, 1971.
- [30] Fabrizio Grill, Helena Pais, Constan ça Providência, Isaac Vidaña, and Sidney S. Avancini. *Phys. Rev. C*, 90:045803, Oct 2014.
- [31] C.J. Horowitz and Brian D. Serot. *Nucl. Phys. A*, 368(3):503 – 528, 1981.
- [32] J.D. Walecka. *Ann. Phys.*, 83:491–529, January 1974.
- [33] J. Boguta and A.R. Bodmer. *Nucl. Phys. A*, 292(3):413–428, December 1977.
- [34] R.J. Furnstahl, Brian D. Serot, and Hua-Bin Tang. *Nucl. Phys. A*, 598(4):539 – 582, 1996.
- [35] R.J. Furnstahl, Brian D. Serot, and Hua-Bin Tang. *Nucl. Phys. A*, 615(4):441 – 482, 1997.
- [36] B. Kumar, S.K. Singh, B.K. Agrawal, and S.K. Patra. *Nucl. Phys. A*, 966:197 – 207, 2017.
- [37] Shailesh K. Singh, S. K. Biswal, M. Bhuyan, and S. K. Patra. *Phys. Rev. C*, 89:044001, Apr 2014.
- [38] Brian D. Serot and John Dirk Walecka. *Adv. Nucl. Phys.*, 16:1–327, 1986.
- [39] J. Boguta and A. R. Bodmer. *Nucl. Phys. A*, 292(3):413–428, December 1977.
- [40] S. Typel and H.H. Wolter. *Nucl. Phys. A*, 656:331–364, 1999.
- [41] G. A. Lalazissis, J. König, and P. Ring. *Phys. Rev. C*, 55:540–543, Jan 1997.
- [42] Y. Sugahara and H. Toki. *Nucl. Phys. A*, 579:557–572, 1994.
- [43] C. J. Horowitz and J. Piekarewicz. *Phys. Rev. C*, 64:062802, Nov 2001.
- [44] B. G. Todd-Rutel and J. Piekarewicz. *Phys. Rev. Lett.*, 95:122501, Sep 2005.
- [45] F. J. Fattoyev, C. J. Horowitz, J. Piekarewicz, and G. Shen. *Phys. Rev. C*, 82:055803, Nov 2010.
- [46] G. A. Lalazissis, T. Nikšić, D. Vretenar, and P. Ring. *Phys. Rev. C*, 71:024312, Feb 2005.
- [47] X. Roca-Maza, X. Viñas, M. Centelles, P. Ring, and P. Schuck. *Phys. Rev. C*, 84:054309, Nov 2011.
- [48] Arianna Carbone and Achim Schwenk. *Phys. Rev. C*, 100:025805, Aug 2019.
- [49] J. R. Oppenheimer and G. M. Volkoff. *Phys. Rev.*, 55:374–381, Feb 1939.
- [50] Richard C. Tolman. *Phys. Rev.*, 55:364–373, Feb 1939.
- [51] Luciano Rezzolla, Elias R. Most, and Lukas R. Weih. *Astrophys. J.*, 852(2):L25, jan 2018.
- [52] B. Margalit and B. D. Metzger. *Astrophys. J.*, 850(2):L19, nov 2017.
- [53] Nai-Bo Zhang and Bao-An. Li. *Eur. Phys. J. A*, 55:1434–601X, Mar 2019.
- [54] S. S. Bao, J. N. Hu, Z. W. Zhang, and H. Shen. *Phys. Rev. C*, 90:045802, Oct 2014.
- [55] S. S. Bao and H. Shen. *Phys. Rev. C*, 89:045807, Apr 2014.